Visual Cycle: Dependence of Retinol Production and Removal on Photoproduct Decay and Cell Morphology

Petri Ala-Laurila,[1] Alexander V. Kolesnikov,[2] Rosalie K. Crouch,[3] Efthymia Tsina,[4] Sergey A. Shukolyukov,[2] Victor I. Govardovskii,[2] Yiannis Koutalos,[3] Barbara Wiggert,[5] Maureen E. Estevez,[1] and M. Carter Cornwall[1]

[1]Department of Physiology and Biophysics, Boston University School of Medicine, Boston, MA 02118
[2]Institute for Evolutionary Physiology and Biochemistry, Russian Academy of Sciences, 194223 St. Petersburg, Russia
[3]Department of Ophthalmology, Medical University of South Carolina, Charleston, SC 29425
[4]Department of Ophthalmology, Agia Sophia Children's Hospital, University of Athens, Athens 11527, Greece
[5]National Eye Institute, National Institutes of Health, Bethesda, MD 20892

The visual cycle is a chain of biochemical reactions that regenerate visual pigment following exposure to light. Initial steps, the liberation of all-trans retinal and its reduction to all-trans retinol by retinol dehydrogenase (RDH), take place in photoreceptors. We performed comparative microspectrophotometric and microfluorometric measurements on a variety of rod and cone photoreceptors isolated from salamander retinae to correlate the rates of photoproduct decay and retinol production. Metapigment decay rate was spatially uniform within outer segments and 50–70 times faster in the cells that contained cone-type pigment (SWS2 and M/LWS) compared to cells with rod-type pigment (RH1). Retinol production rate was strongly position dependent, fastest at the base of outer segments. Retinol production rate was 10–40 times faster in cones with cone pigments (SWS2 and M/LWS) than in the basal OS of rods containing rod pigment (RH1). Production rate was approximately five times faster in rods containing cone pigment (SWS2) than the rate in basal OS of rods containing the rod pigment (RH1). We show that retinol production is defined either by metapigment decay rate or RDH reaction rate, depending on cell type or outer segment region, whereas retinol removal is defined by the surface-to-volume ratio of the outer segment and the availability of retinoid binding protein (IRBP). The more rapid rates of retinol production in cones compared to rods are consistent with the more rapid operation of the visual cycle in these cells.

INTRODUCTION

Photon absorption by a visual pigment within rod and cone photoreceptors produces a cis-to-trans isomerization of its retinal chromophore, resulting in an activation of the visual pigment (R* or metarhodopsin II). This initial photochemical event triggers the activation of the visual transduction cascade that eventually leads to transmission of a visual signal from the photoreceptor to other cells within the retina and thence to the brain. Once the chromophore has undergone photoisomerization, the visual pigment is said to be "bleached," i.e., it is no longer able to absorb photons in the "visual" region of the spectrum. The regeneration of the visual pigment to its previous dark state occurs by a series of biochemical reactions referred to as the visual cycle. The initial steps in the visual cycle occur immediately following photon absorption and appearance of the active form of the visual pigment. These initial steps are slow thermal reactions that result in separation of the all-trans retinal chromophore from opsin, the apoprotein portion of the visual pigment, followed by the reduction of all-trans retinal to all-trans retinol. All of these steps occur within the photoreceptor outer segment. Beyond this point, the visual cycle for rod and cone photoreceptors appears to diverge. In rods, retinol translocates from the outer segment via the intercellular matrix to the retinal pigment epithelium, where it is subjected to a multistep enzymatic conversion to 11-cis retinal. After this regenerative isomerization, the 11-cis retinal chromophore is translocated back to rod outer segments, where it condenses with the apoprotein to regenerate the dark visual pigment. In cones, recent work has proposed that all-trans retinol is likely to translocate from outer segments to Müller cells, where enzymatic isomerization to 11-cis retinol is suggested to occur (Mata et al., 2002, see also Das et al., 1992). It is proposed that after transfer of this chromophore back to cones, oxidation of the retinol to retinal is followed by recombination of retinal with opsin to form the dark visual pigment.

P. Ala-Laurila and A.V. Kolesnikov contributed equally to this work.
Correspondence to Petri Ala-Laurila: pal@bu.edu

Abbreviations used in this paper: IRBP, interphotoreceptor retinoid binding protein; IS, inner segment; LED, light-emitting diode; MSP, microspectrophotometry; NADPH, nicotinamide adenine dinucleotide phosphate (reduced form); OS, outer segment; PSB, protonated Schiff base; RAL, retinal; RDH, retinol dehydrogenase; ROL, retinol; ROS, rod outer segment.

It is well known that under normal bright daylight conditions, rod photoreceptors are unresponsive to light, and our visual system relies substantially, if not exclusively, on cones to transmit visual images to the brain. This is in large part due to biochemical and physiological differences within rod and cone outer segments that regulate their flash sensitivity, as well as differences in recovery mechanisms during and following exposure to varying levels of background light. For instance, cones of cold-blooded vertebrates (salamander) recover sensitivity following bright bleaching light ∼10-fold faster than do rods of the same species (Jones et al., 1989; Jones et al., 1993). Similarly, in man, both classical psychophysical results and recent work comparing human rod and cone ERGs show that the recovery of sensitivity after massive bleach takes in cones 1–2 min, whereas in rods it needs ∼20 min (Thomas and Lamb, 1999; Mahroo and Lamb, 2004).

Difference in the rates of recovery may be related to a difference in the way rods and cones handle the photoproducts of bleaching, in particular, all-trans retinal. This idea is based on two important observations. First, exposure of photoreceptors to bright light results in the persistence of metaproducts and leads to a prolonged activation of the transduction cascade that limits recovery of sensitivity (for review see McBee et al., 2001). Second, all-trans retinal can combine in vitro with opsin to form complexes that have significant G-protein activity (Fukada and Yoshizawa, 1981; Cohen et al., 1992; Surya et al., 1995; Jäger et al., 1996), thereby maintaining the activity of the transduction cascade at a high level. Thus, reduction of retinal to retinol may be necessary for the quenching of the catalytic activity. In addition, experiments have shown that the reduction of retinal to retinol under some circumstances may be rate limiting in the visual cycle (Saari et al., 1998). The idea is also consistent with biochemical studies (Palczewski et al., 1994; Rattner et al., 2000), both of which implicate the possible involvement of outer segment retinol dehydrogenase (RDH) in limiting the rate of response recovery by perhaps regulating the activities of transducin, rhodopsin kinase, arrestin, or the rate of pigment regeneration.

The large differences in the rate of pigment regeneration and response recovery that have been observed in rods and cones could derive from a variety of factors. Principal among these are (1) different rates of liberation of retinal following metapigment decay in different cell types, and (2) differences in the intrinsic rates of cone versus rod retinal dehyrogenases (RDHs). Some measurements of differences in RDH activity have been documented in cone-rich and rod-rich retinae (Mata et al., 2002). However, no systematic characterization of the intrinsic rod and cone RDH activities has yet been undertaken. Thus, is it not clear to what extent differences in RDH rate may explain the observed large differences in cone vs. rod recovery. Whether such rod/cone differences in recovery rate may be due to differences in photoproduct decay rate has never been investigated either. Thus, the primary goal of the present study was to measure the rates of photoproduct decay in rods and cones and to determine the extent to which these rates contribute to different rates of retinol production. A second goal was to measure rates of retinol clearance in these same photoreceptor outer segments following bleaching and to determine what relationship may exist between the observed clearance rates of retinol and different outer segment morphologies.

In this study, we employed microfluorometry and microspectrophotometry of intact, isolated salamander photoreceptors to characterize the time courses of metarhodopsin decay and all-trans retinol production in various types of rods and cones that differ in their pigment type and morphology. These cell types were red and green rods in which the pigments (RH1 and SWS2, respectively) are contained in internal disk membranes and red- and blue-sensitive cones in which the pigments (L/MWS and SWS2) are contained in the plasma membrane (see Ebrey and Koutalos, 2001, for a discussion of the classification of visual pigment types).

We applied a simple kinetic scheme of retinal-to-retinol conversion to the data to define the rate-limiting step(s) of retinol production in each cell type. Our analysis shows that the rate of retinol production is defined either by the metapigment decay rate or the RDH reaction rate. Either of these can be the rate-limiting step of retinol production depending on the cell type and the OS region. Results showed that metarhodopsin decay rate limited retinol production only at the basal OS of salamander red rods with the RH1 pigment. In all other cell types and OS regions, the rate-limiting step was the RDH reaction. We hypothesize that the modulatory step that rate limits the RDH reaction is the limited supply of the RDH cofactor NADPH. Further, we show that retinol removal is defined by the surface-to-volume ratio of the outer segment.

MATERIALS AND METHODS

Animals and Preparation
Experiments were performed on red- and blue-sensitive cones, and red and green rods of larval tiger salamanders (*Ambystoma tigrinum*). Larval salamanders were purchased from Charles D. Sullivan Company, Inc. and kept at ∼10°C in aquarium tanks on a 12-h light/12-h dark cycle.

Salamanders were dark adapted overnight at room temperature before each experiment. Intact photoreceptors were mechanically isolated from dark-adapted retinae under infrared illumination as described previously (Cornwall et al., 1990; Tsina et al., 2004). All procedures were performed according to protocols approved by the Animal Care and Use Committee of Boston University School of Medicine and in accordance with the standards set forth in the Guide for the Care and Use of Laboratory Animals and the Animal Welfare Act.

Solutions

The Ringer solution used for dissection of retinae and superfusion of photoreceptors had the following composition (in mM): 110 NaCl, 2.5 KCl, 1.6 MgCl$_2$, 1.0 CaCl$_2$, 10 dextrose, 10 HEPES, pH 7.8. The Ringer solution also contained 1.5 µM BSA.

Microfluorometry

After dissection, a suspension of cells in physiological solution containing intact rods and cones was placed in a recording chamber located on the stage of an inverted microscope (ECLIPSE TE300, Nikon). The microscope was equipped for use in conventional epi-fluorescence mode. An infrared-sensitive TV camera and an infrared light source were attached to the microscope optical system to allow bright-field viewing of the cells in the chamber during experiments.

Microfluorometric measurements of changes in intrinsic fluorescence within outer segments of photoreceptors were made on dark-adapted cells after bleaching with bright light. Measurements of increases in intrinsic fluorescence within bleached rod outer segments have been shown previously to be due to the appearance of all-trans retinol after its reduction from all-trans retinal (Liebman, 1969; Tsina et al., 2004; Chen et al., 2005). Light for fluorescence excitation of the cells entered the microscope via the fluorescence port from a Xenon continuous arc (Optosource Arc Lamp and power supply, Cairn Instruments, Ltd.). Prior to entering the microscope, this light was passed through neutral density filters (Chroma Technology), a 360-nm narrow-band interference filter (Chroma Technology), and an electronic shutter (Vincent Associates). The beam of light was reflected upward by a dichroic mirror (4000DCLP, Chroma Technology) and focused through a microscope objective (Nikon 100X S Fluor, Nikon) onto the plane at which the cells were located within the recording chamber. Cells within the recording chamber were continuously superfused with Ringer solution. The flow rate of the superfusate was controlled by gravity and was ∼1.0 ml/min. In the experiments where the effect of interphotoreceptor retinoid binding protein (IRBP) was tested, 100 µM IRBP was added directly to the physiological solution in the recording chamber. The temperature of the superfusate solution in the recording chamber was maintained at 22 ± 1.0°C.

Exposure of individual photoreceptors to a 200–800-ms step of excitation light resulted in fluorescence emission from the cells. The fluorescence light was collected by the microscope objective, passed through the dichroic filter and a wide-band emission filter (pass band 465 nm–550 nm, D510/80M, Chroma Technology), and focused on the face of an image intensifier (VS4-1845; Videoscope International, Ltd.). Images were captured using a CCD camera (CoolSNAP fx; Roper Scientific, Inc.; Photometrics). The output of the camera was used to produce bright-field images and pseudocolor fluorescence images, as illustrated in Fig. 1. Using this method, the spatial and temporal changes in the distribution of fluorescence were measured before and at different times after exposure to a bright bleaching light. Data acquisition was performed using Openlab 3.0 (Improvision, Inc.). Digitized images were stored on a computer hard drive for later processing.

Light Stimulation and Pigment Bleaching

An optical stimulator provided light stimuli for visual pigment bleaching in microfluorometric recordings as well as for test flashes used for electrophysiological recordings (Tsina et al., 2004). The stimulator focused a light spot of 400 µm diameter and uniform intensity at the plane of the preparation through a 10× microscope objective mounted in the condenser holder of the inverted microscope. At the beginning of each experiment, the unattenuated intensity of light passed through a 520-nm interference filter (10-nm half band) was adjusted to a value of 7.1×10^7 photons µm^{-2}s^{-1} with a calibrated photometer (United Detector Technology, Model 80X). The wavelength of light stimulation for each receptor type was selected to be near the wavelength of maximum sensitivity of that type: 520 nm (red rods), 440 nm (green rods and blue-sensitive cones), and 620 nm (red-sensitive cones). The intensity of light at these other wavelengths was measured periodically to see that systematic changes did not occur.

The fraction of visual pigment bleached (F) was calculated according to the relation:

$$F = 1 - \exp(-IP_\lambda t), \qquad (1)$$

where I is the absolute light intensity at the selected wavelength (photons µm^{-2}s^{-1}), P_λ is the photosensitivity at the wavelength of the stimulus light (µm^2), and t is the duration of the light exposure (s). The value that we used for the photosensitivity of red and green rods, as well as red- and blue-sensitive cones at the wavelength of peak absorbance, was $P_\lambda = 6 \times 10^{-9}$ µm^2 (Jones et al., 1993; Cornwall et al., 2000). In all fluorescence experiments, we used bleaching intensities and exposure times that were calculated to have bleached >90% of the pigment.

Identification of Cell Types

Salamander retina contains two different types of rod photoreceptors with visual pigments embedded in closed discs ("red" rods and "green" rods) and three different types of cone photoreceptors with visual pigments embedded in the plasma membrane (UV-sensitive cones, blue-sensitive cones, and red-sensitive cones) (Hárosi, 1975; Cornwall et al., 1984; Mariani, 1986; Makino and Dodd, 1996; Sherry et al., 1998). Salamander green and red rods were identified morphologically, based on the size and shape of their OSs and ellipsoid regions. Green rods have elongated ellipsoid regions, and the OSs are typically shorter than those of red rods (Mariani, 1986; Ma et al., 2001; see also the bright field images, Fig.1).

Salamander red-sensitive cones and blue-sensitive cones were identified before bleaching using electrophysiological criteria by measuring the relative amplitude of their flash responses to 440-, 520-, and 620-nm light stimuli. These measurements were made by drawing the inner segment/ellipsoid portion of each of the cells into a close-fitting glass micropipette that was connected to a patch clamp amplifier (EPC-7, List Associates) and the photocurrent was recorded extracellularly. This suction pipette technique for recording of photocurrent responses to measure cell sensitivity has been described previously (Baylor et al., 1979; Cornwall et al., 1990). The photocurrent signal was low-pass filtered at 20 Hz, digitized at 100 Hz, and stored on a computer hard drive for later analysis. Data acquisition and analysis were performed using pCLAMP 8 software (Axon Instruments).

Analysis of Fluorescence Images

The average fluorescence intensity was calculated in different parts of the cells by establishing regions of interest based on bright field images of the cells obtained during the fluorescence experiments (see Tsina et al., 2004). These regions were the inner segment containing the nucleus, the ellipsoid region containing numerous mitochondria, and different regions within the OS. To study the spatial differences in OS fluorescence, the OS was divided into several regions of similar longitudinal size. The average fluorescence was calculated in each region and corrected for background fluorescence measured within the region before bleaching. Interphotoreceptor differences were evaluated by comparing changes in the averaged fluorescence intensity in regions of approximately similar longitudinal size measured in the most proximal region of rod OSs. Comparisons in cones were made based on measurements in the whole OSs as well as in regions. The analyses of fluorescence images were performed using Openlab 3.1 software (Improvision, Inc.) and Origin 6.1 (OriginLab Co.).

Microspectrophotometric Analysis of Photolysis

The time course of photolysis of visual pigments was studied with a high-speed dichroic microspectrophotometry (MSP) instrument described earlier (Govardovskii and Zueva, 2000; Kolesnikov et al., 2003). The microspectrophotometer was equipped with a computer-controlled jumping beam mask that allowed fast sequential recordings from tip and base of the same rod outer segment. The mask had a changeable width and a fixed length of 8 μm; its longitudinal excursion (with respect to the rod outer segment [ROS] long axis) can be adjusted to place the measuring beam in different positions along the ROS. The solution used for measurements was identical to the one used in electrophysiological and microfluorometric measurements.

In most cases, measurements were performed on retinal samples placed in a superfusion chamber that consisted of a well ∼2 mm in depth, with the bottom made of a microscope coverslip. Solution was fed to the chamber by gravity; outflow was removed by suction. A water immersion objective (58×, 0.8 NA UV, Leningrad Optical-Mechanical Factory) was used for sample viewing and light collection. Recordings were made from intact isolated photoreceptors, isolated outer segments, or intact photoreceptors whose outer segments protruded from a retinal fragment. Sometimes measurements were made from nonperfused samples contained in a sealed chamber.

For baseline recording, the measuring beam was first placed in a cell-free space near the cell to be measured, and baseline intensities were recorded at two beam polarizations and slit positions used for spectral scans. The axis of polarization of the measuring light was either in the transverse direction (orthogonal to the long axis of the outer segment, hereafter labeled T) or in the longitudinal direction (parallel to the outer segment, hereafter labeled L). T-scans were made from longer to shorter wavelengths and L-scans in the reverse direction. A full spectral scan at a given slit position and two polarizations took from 0.9 to 1.1 s, depending on the spectral range. After averaging four baseline scans at each polarization and position, the beam was placed on the outer segment, and absorbance spectra were recorded. The time lapse between scans at two slit positions was 50 ms. Then the visual pigment was bleached with a flash of 1,000–1,500 ms duration from a high-intensity light-emitting diode (LED), and a series of post bleach spectra recorded at predefined time intervals. The LEDs used for bleaching had peak emissions at 615 nm (for red-sensitive cones), 525 nm (for red rods), and 465 nm (for green rods) (Marl International). The flash exposure was sufficient to bleach the visual pigment to a photoequilibrium state. The small fraction of unbleached and photoregenerated pigment was determined by applying a second exhaustive bleach after complete decay of metaphotoproducts, as previously described (Kolesnikov et al., 2003).

Processing of MSP Data

Raw MSP spectra from several cells were averaged to reduce noise. Correction for nonspecific absorbance and light scattering was made by fitting a straight line by the method of least-squares to the long-wavelength portion of the spectrum, where absorbance of the visual pigment is negligible. This region was either between 700 and 800 nm or between 600 and 800 nm, depending on the wavelength of peak sensitivity (λ_{max}) of the pigment. Differences between these derived values and zero absorbance were then subtracted from the raw spectrum to produce a baseline corrected spectrum. Next, the spectrum of the unbleached pigment fraction was subtracted. The resulting spectrum was used to calculate the composition of the mixture of photoproducts.

Generally, after bleaching, six spectrally distinct long-lived photoproducts were observed. These are metarhodopsin I, II, and III (meta I, II, and III), all-trans retinal/dehydroretinal, nonspecific protonated Schiff bases of retinal (PSBs), and all-trans retinol/dehydroretinol. The analysis of the mixture is facilitated by the fact that meta I and II are in a rapid equilibrium, so from a kinetic standpoint they can be considered as a single product, hereafter referred to as M. Thus, five coexisting products with largely overlapping spectra can be considered, namely M, meta III, all-trans retinal, its PSBs, and all-trans retinol. T- and L-absorbances of retinol were treated separately, which added the sixth variable. Spectrally similar products (M and all-trans retinal, or meta III and retinal Schiff bases) have different orientations of their chromophores with respect to the disk plane. Therefore, measurements of absorbances at three wavelengths and two polarizations can be analyzed by a system of six linearly independent equations whose solutions yield the contribution of each product to the recorded spectra. The wavelengths for measurements were chosen to lie close to absorbance maxima of main products. They were 340 nm (isosbestic point of retinol/dehydroretinol), 390 nm (isosbestic point of retinal/dehydroretinal), and 470–490 nm (near MIII and PSB maxima, depending on the chromophore composition; see below). Since the noise in the short-wave region around 340 nm is high, retinol absorbances found this way were rather inaccurate. To refine the result, absorbances of M, meta III, PSB, and retinal (RAL) were subtracted from the experimental spectrum to obtain the remaining T- and L-spectra of all-trans retinol. Their amplitudes were then determined by the least-square fit with the standard retinol template. This approach is described in more detail by Kolesnikov et al. (2003) and Golobokova and Govardovskii (2006).

The analysis of MSP data is complicated by the fact that larval tiger salamanders contain a mixture of two visual pigment chromophores: 11-cis retinal (A1) and 11-cis-3-dehydroretinal (A2). Chromophoric composition was determined in each animal by fitting the dark-adapted spectra with a combination of A1/A2 visual pigment templates (Govardovskii et al., 2000). Corresponding mixtures of standard retinal/dehydroretinal and retinol/dehydroretinol spectra were then used in further computations. To establish the template for M formed by a mixture of A1- and A2-based metapigments, we fitted the T- and L-absorbance recordings at 1.5 s post-bleach with a sum of two Gaussians. It usually provided an excellent approximation. As for the templates for Meta III and PSB, their exact shape is not crucial for finding concentrations of all photolysis products. Only the absorbances at the wavelengths of measurements (340 and 390 nm) relative to their maxima at 470–490 nm are required. These relative absorbances were taken as 0.25 (Meta III both at 390 and 340 nm; Kolesnikov et al., 2003), 0.54 (PSB at 390 nm), and 0.23 (PSB at 340 nm; Morton and Pitt, 1955; Pitt et al., 1955), as in A1-based pigments. Since these values characterize minor components, their uncertainty does not substantially influence the results.

Surface to Volume Ratio Estimates

The estimates of the surface to volume ratio for each cell type were based on the bright field images taken during fluorescence recordings. For each cell, the radius of the OS in the proximal (R), the distal (r) regions, as well as the total length of the OS (L) were measured (see Table I). The volume (V) and the total surface area of the cell (S) were calculated by estimating the cone OS as a frustum of a right circular cone. Under these assumptions:

$$V = \pi \cdot L/3 \cdot (R^2 + r \cdot R + r^2) \tag{2}$$

and

$$S = \pi \cdot ((R - r)^2 + L^2)^{1/2} \cdot (r + R) + \pi \cdot r^2. \tag{3}$$

We estimated rod OSs as cylinders. The surface to volume ratio estimates (S/V) for rods were then obtained by substituting $r = R$ in the above formulas. This simple approach for the surface to volume ratio calculations does not take into account the additional

surface area of membrane invaginations found in cone outer segments (see Discussion for consideration of cone invaginations).

RESULTS

Distribution of Retinol Fluorescence in Bleached Photoreceptors

A significant advantage to the use of the microfluorometric technique is that it provides detailed measurements of the spatial profile as well as the kinetics of production of retinol within bleached rod and cone photoreceptors. Measurements of this kind are illustrated in the four columns of pseudocolor images displayed in Fig. 1 A. These images compare the spatial and temporal changes in intrinsic fluorescence that occur in the inner and outer segments of a variety of intact rod and cone photoreceptors after exposure to a bright light that bleached >90% of the visual pigment.

These cells were chosen to be representative of three classes of photoreceptors, differentiated based on their cellular morphology and their visual pigment content. Red rods (RR, far left column) contain rhodopsin pigment (RH1) primarily in internal disc membranes. Green rods (GR, second from left) contain pigment in internal discs, but this pigment belongs to the cone pigment family (SWS2) (Ma et al., 2001). Blue-sensitive cones (BC, second from right) and red-sensitive cones (RC, far right) contain cone pigments (SWS2 and M/LWS, respectively) embedded in infoldings of the plasma membrane (Mariani, 1986; Sherry et al., 1998; Ma et al., 2001). At the top of each column is a bright field image of a representative of each cell type. Each of these is shown at the same scale and in the same orientation: the inner segment (IS) of each cell is on the left side of each panel and the outer segment (OS) on the right. The ISs of blue- and red-sensitive cones are shown drawn into glass recording micropipettes in order that they could be discriminated from one another by electrophysiological criteria (see Materials and Methods). Below each bright field image is a column of five pseudocolor fluorescence images. The top image was taken before exposure to bright bleaching light; the bottom four images were measured at different times following the bleach. Fluorescence intensities are coded by different colors (see the color bar in Fig. 1). Together, these images illustrate the different rates at which retinol fluorescence first increased in the OSs after the exposure to bright light and later decreased as retinol was cleared in these different cell types. Spatial and temporal increases of retinol fluorescence that are qualitatively similar to those shown in Fig. 1 have been observed previously in bleached frog rods (Liebman, 1969, 1973; Chen et al., 2005) and in salamander red rods (Tsina et al., 2004). Based on the spectrum and the polarization of the fluorescence light, the fluorescence increase in the OS after

bleaching in these cells has been attributed to the production of all-trans retinol, and the spatially localized fluorescence in the ellipsoid region has been attributed to substances other than retinol, presumably to reduced nicotinamide adenine dinucleotide phosphate (NADPH) (Liebman, 1969; Tsina et al., 2004; Chen et al., 2005).

Before bleaching occurred, fluorescence levels within outer segments of all of the cells were generally very low. The fluorescence levels in the inner segment (ellipsoid) regions of the cells, which contain mitochondria, were somewhat higher and changed little after exposure to bleaching light. However, after bleaching, a large and spatially nonuniform increase in fluorescence was observed to develop in the OSs of all the cells. As shown by the fluorescence recordings in red and green rods (see first two columns of Fig. 1 A), the fluorescence increased fastest in the most proximal part of the OS and slowest in the most distal part of the OS.

Fig. 1 B shows the time course of changes in the normalized relative fluorescence levels in the whole OS for each of the cells shown in A. The same acronyms (RR, GR, etc.) are used as in A. The five data points corresponding to the pseudocolor images illustrated in each column in A are highlighted by red squares in the corresponding plots in B, whereas all other data points of the fluorescence measurements that are not shown in A are marked by black symbols. It can be seen from these plots that there is a wide variation in both the kinetics of production and clearance of retinol fluorescence in these different cell types.

The relative fluorescence change averaged over the whole OS reached its maximum in ∼25 min in the red rod, and in ∼4 min in the green rod (see Fig. 1, A and B, RR and GR). In salamander cones, the fluorescence increase in the OS is significantly faster than in either of the rods and reaches its maximum value within 1–2 min in both red- and blue-sensitive cones, as shown by the two rightmost columns of A and the corresponding plots in B. The clearance of fluorescence is also significantly faster in salamander cones than in the rod photoreceptors. As shown in B, 50% of the relative fluorescence was cleared in both the red- and the blue-sensitive cones in ∼9 min, whereas in both of the rods illustrated in Fig. 1, the same level of clearance occurs only on the time-scale of 2–3 h.

Wave-like Spread of Retinol Fluorescence

Data illustrated in Fig. 2 A as well as results reported earlier (Tsina et al., 2004) demonstrate that the retinol fluorescence observed following bleaching of salamander red rods increases initially in the proximal region of the OS (open squares) and last in the distal region (filled squares). A qualitatively similar wave-like spatial spread of retinol fluorescence was also observed in green rods as well as both of the cone types.
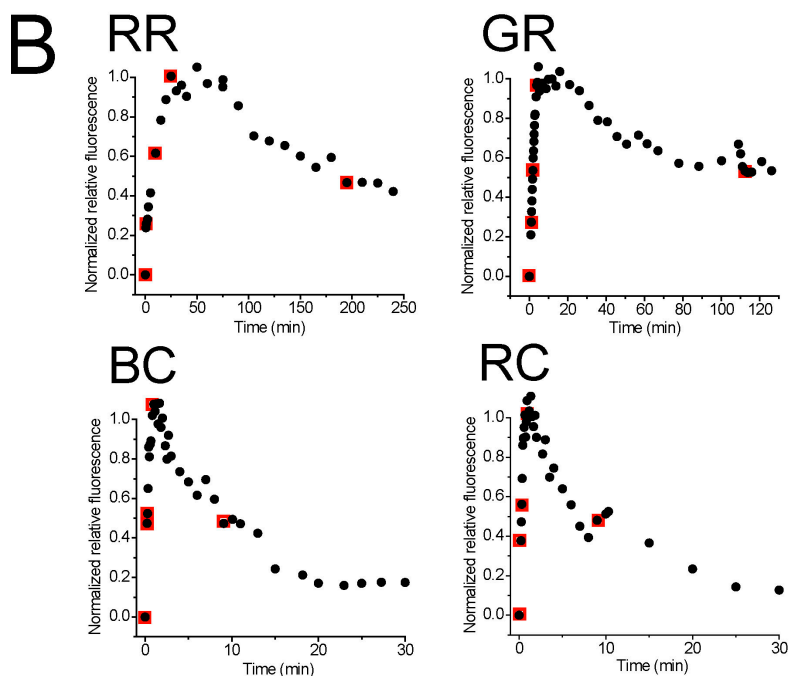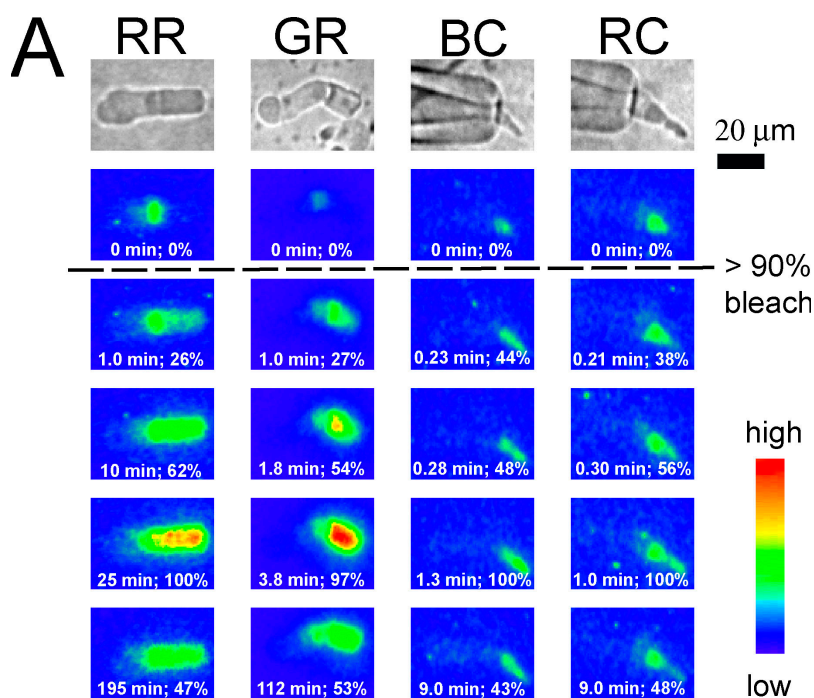
Ala-Laurila et al.   157

Figure 1. Bright field and pseudo-color fluorescence images before and after bleaching the visual pigment of salamander rod and cone photoreceptor cells. (A) The top row shows bright field images of single photoreceptor cells: (from left to right) red rod (RR), green rod (GR), blue-sensitive cone (BC), and red-sensitive cone (RC). The five pseudo-color images shown below each bright field image were measured before (top) and at different times after exposure to a bright light (at time = 0) that bleached >90% of the visual pigment. The time at which the image was taken and the normalized relative fluorescence (%) averaged over the whole OS are shown at the bottom of each fluorescence image. (B) Plots of the time course of the average normalized relative fluorescence intensity for each of the cells shown in A. The five data points highlighted by red squares correspond to the fluorescence images shown in A. Data points from fluorescence images not illustrated in A are indicated by black circles.

The graphs shown in Fig. 2 B illustrate an example of this wave-like behavior in red-sensitive cones. The two plots in the main panel show the time course of fluorescence change after exposure to bright light in two regions of roughly similar longitudinal size (3–4 μm) within the outer segments of six intact cones. The plot composed of the open squares illustrates the fluorescence increase measured in the most proximal region of the outer segment; the filled squares illustrate the fluorescence increase at the distal tip. The inset shows the same data as in the main panel plotted on an expanded time scale. The lower amplitude of relative fluorescence observed at the tip of the OS can be explained purely based on geometrical considerations, i.e., the peak level of fluorescence depends on the average thickness of the OS in this region. Here, the overall average thickness of the OS at the tip is much smaller than at the base. However, when correction for compartment thickness is made, it is also apparent that the fluorescence signal rises more slowly at the tip of the OS than at the base.
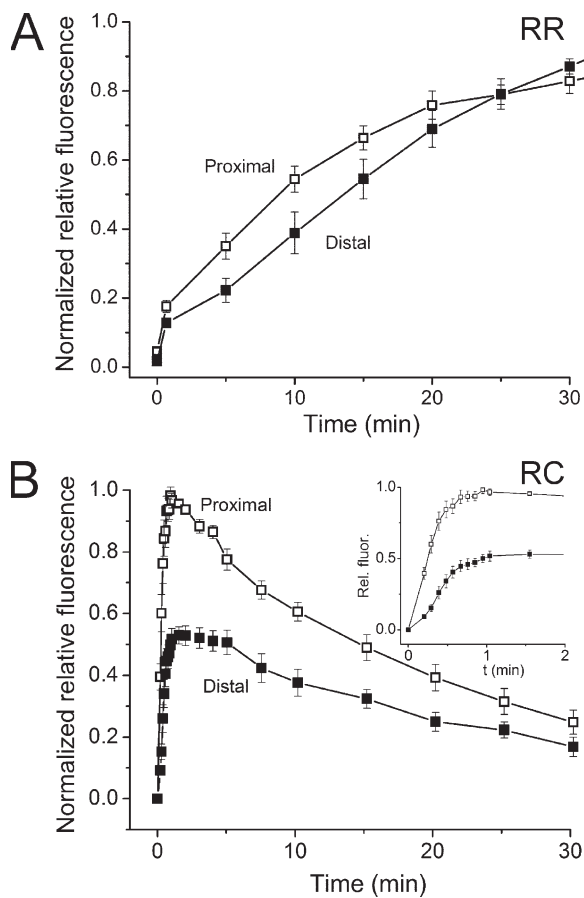
Figure 2. Time course of the average normalized fluorescence change (mean ± SEM) in two different outer segment regions of intact isolated salamander red rods ($n = 7$, A) and red-sensitive cones ($n = 6$, B): proximal OS (□), distal OS (■). (B, inset) Same data as in main panel plotted on expanded time scale. Data are normalized relative to the peak value.
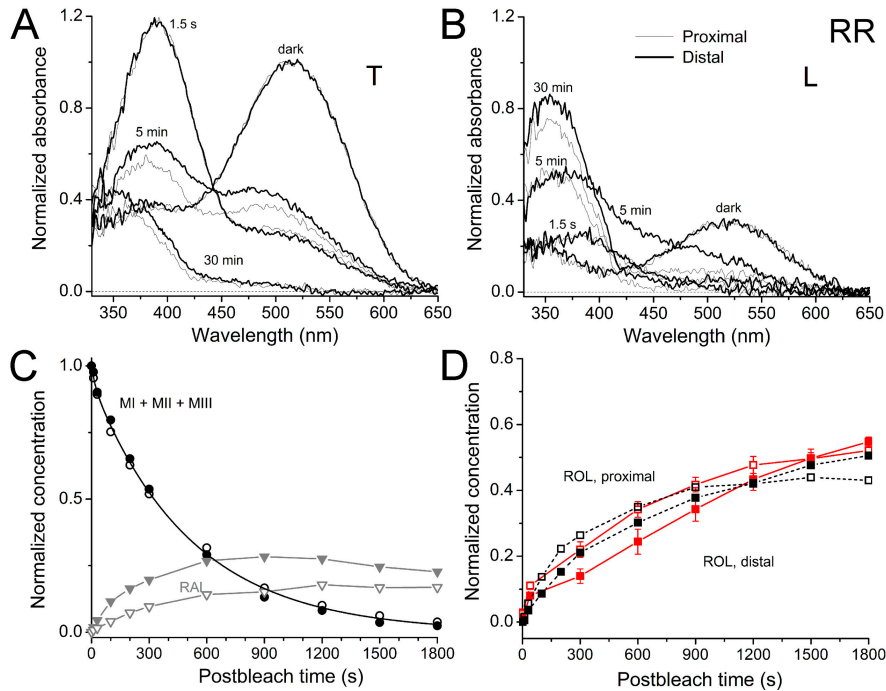
Metarhodopsin Decay Rate and Retinal Release As Assessed by Microspectrophotometry

It is apparent from the fluorescence data presented in Fig. 1 that the rate of retinol production is grossly different among different cell types. It is also clear from measurements within the different regions of the same outer segment (Fig. 1 A; Fig. 2) that these production rates also differ widely. An important question is whether these differences result from different rates of liberation of all-trans retinal that serves as a substrate for the RDH reaction or from differences in the speed of retinal reduction. Microfluorometric measurement of retinol fluorescence is a useful tool to measure the differential rates of production of retinol, but this technique provides no direct information about the rate of retinal production. For this we made microspectrophotometric measurements of the kinetics of metaproduct decay in bleached photoreceptor outer segments to determine the rate at which the retinal substrate was produced.

We first tested whether there is a regional difference in the metaproduct decay rate within the same outer

segment. MSP measurements were conducted on salamander red and green rods, since the large size of their outer segments allows accurate positioning of the measuring beam at two locations within the OS. Fig. 3 (A and B) shows the results when measurements are made with T and L polarizations (see Materials and Methods) at the base and tip of salamander red rods. Recordings from the tip are shown by bold lines; measurements at the base are indicated by thin lines. The spectra are normalized to unity at the spectral maximum of the dark pigment. It is apparent from these spectra that immediately after the bleaching exposure, the main peak of the pigment disappears and a mixture of meta II (peak at ~390 nm) and meta I (shoulder near 475 nm) is generated. This is best seen in T polarization spectra (see the curve labeled 1.5 s in Fig. 3 A). A progressive decrease of the magnitude of the 390-nm peak is evidence for meta I/II decay, while the transient increase of the absorbance at 475 nm indicates the appearance and subsequent decay of meta III (curves at 5 min). Further changes in the absorbance spectra demonstrate a gradual conversion of retinal to retinol. This is seen from the loss of absorbance in the 425–600-nm region of the spectrum and the appearance of the sharp peak at ~350 nm (best shown by the curve at 30 min in Fig. 3 B). It is evident from inspection that reduction of retinal to retinol at the ROS tip proceeds substantially slower than at its base. At 5 min post bleach, long wavelength–absorbing substances (retinal and PSBs) are present in significantly higher concentrations at the tip, and their conversion to retinol is incomplete even at 30 min.

As explained in Materials and Methods, measurements at two polarizations and three wavelengths allow the computation of the time courses of absorbance changes of all main products (M, MIII, RAL, ROL, and PSB). Fig. 3 (C and D) illustrates the result of such calculations based on the data shown in A and B. Fig. 3 C shows a comparison between the time course of metarhodopsin decay (circles) and retinal (triangles) concentrations at the tip (filled symbols) and the base (open symbols) of the outer segments. Throughout this paper, concentrations of photoproducts are normalized to the concentration of the bleached visual pigment. This means that the calculations yield concentrations expressed as a fraction of the bleached pigment, i.e., the metaproduct curve starts from unity because immediately after the bleach all of the visual pigment has been converted to the M form, and no other product is present. Calculations show that the decay of the sum of metaproducts (MI+MII+MIII), and hence the production of retinal at the ROS tip and base follow identical time courses. This decay is well fitted by a sum of two exponents (continuous black line in C, $r^2 = 0.999$) that corresponds to interconversion and decay of two products, M and MIII (Kolesnikov et al., 2003). It can also be satisfactorily described by a single exponent with a time

Figure 3. Photolysis of salamander red rod visual pigment at the tip and base of the ROS as assessed by microspectrophotometry. (A) Absorbance spectra recorded from the tip (bold lines) and base (thin lines) of salamander red rod (RR) outer segments in darkness, immediately (1.5 s) and at various times after exposure to bleaching light (1500-ms flash, 525-nm). Recordings at 10, 30, 100, 200 s, and 10, 15, 20, and 25 min are omitted from the figure for clarity. Measurements made at T-polarization, average of six cells. (B) Same as A, L-polarization. The spectra are normalized to unity at the T spectral maximum of the bleached pigment at each location. (C) Time courses of concentrations of the sum of metapigments (circles) and retinal (triangles). OS tip, closed symbols. OS base, open symbols. Smooth curve through circles shows a bi-exponential approximation of meta decay based on pooled tip and base data (see Table II for fit parameters). (D) Time courses of retinol production at the ROS base (open squares) and tip (closed squares). Black curves, MSP. Red curves, microfluorometry. Fluorescence data are scaled (by the same factor for base and tip) for best visual match to the MSP data. Error bars represent SEM.

constant of 470 s ($r^2 = 0.997$, not depicted) that we use in further computations (see Discussion). However, retinal accumulates to much higher extent at the tip than at the base of the outer segment owing to the fact that reduction of retinal to retinol proceeds significantly more slowly at the tip than at the base. This is confirmed by the time course of retinol itself (Fig. 3 D). Its concentration at the OS base (empty squares) increases substantially faster than at the tip (filled squares). For comparison, fluorescence data on retinol production (red symbols) are scaled (using the same factor in the tip and base) for best visual fit relative to MSP data (black symbols). The correspondence between the two datasets is reasonable. Together these findings show that the regional differences in retinol production rate along the outer segment do not arise from differences in the rate of metarhodopsin decay but rather at some later stage in retinol production.

Similar measurements were conducted on salamander green rod outer segments. Due to the small proportion of these cells in the salamander retina, we encountered only two intact cells in the MSP samples. The time course of retinol production (dashed lines through black squares in Fig. 4 A) is based on these two cells. However, the decay of metaproducts was also followed on three isolated green rod outer segments that obviously were not capable of converting retinal to retinol. Thus, the meta decay data (solid line through circles in Fig. 4 A) are derived from measurements on five different cells. In agreement with the results on red rods, there was no dif-

ference in the rate of metaproduct decay between the tip and base of the OSs, however, the hydrolysis of the Schiff base linkage between retinal and opsin proceeded ~50-fold faster in green rods than in red rods (time constant of metarhodopsin decay is 9.3 s, Fig. 4 A). It is seen that the difference between the rates of retinol production at the OS tip and base is more pronounced than in red rods. Fluorescence data on five green rods averaged over the entire OS length are in a reasonable agreement with the MSP results (red line through squares in Fig. 4 A).

Plots of retinal and retinol production and clearance in red-sensitive cone outer segments are shown in Fig. 4 B. Cone outer segments are too small for two-position microspectrophotometric recording. Therefore, we made measurements with a single beam that covered 80–90% of the outer segment length. Thus, we have no local MSP data on the visual pigment photolysis in cones. The metaproducts in RC decayed with the time constant of 6.7 s, that is, ~70-fold faster than in red rods. Retinal reached its peak at 20 s after bleach and then declined (gray inverted triangles). Retinol accumulated to 60% of the bleached pigment and then was cleared from the outer segment (black filled squares). Fluorescence data on retinol concentration, when properly scaled, correspond with the MSP curve quite well (filled red squares).

Interphotoreceptor Comparison: Metaproducts Decay, Retinol Production and Clearance

The experiments illustrated in Fig. 5 were designed to determine the effect that pigment type and cell
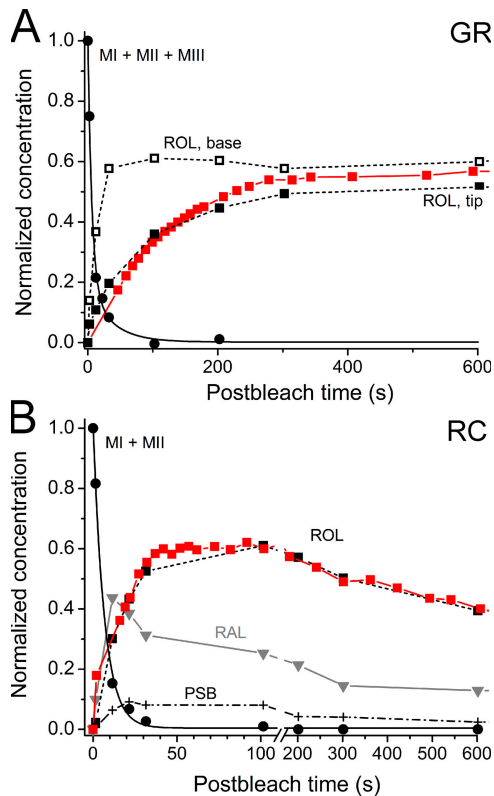
Figure 4. Time course of metapigment decay and retinal and retinol concentration changes in salamander green rods (GR) and red-sensitive cones (RC). Filled circles fitted by black continuous line in A and B illustrate metapigment decay. Parameters of the fits are given in Table II. (A) Black dashed line through black squares, time course of retinol (ROL) as assessed with MSP (filled squares, tip of the OS; empty squares, base). Data on meta decay are average of three isolated OSs and two intact cells; retinol time course deduced from MSP data is based on two intact cells. The retinol time course averaged over entire OS as assessed by microfluorometry (average of seven cells) is shown by red squares. The time courses of retinal and PSB are omitted for clarity. (B) Gray line through inverted triangles shows RAL. Dot-dashed line through crosses, PSB. Average of seven cells. Red line through filled red squares, average time course of retinol (ROL) as assessed with microfluorometry and scaled for the best match to ROL data assessed by MSP. Error bars omitted for clarity.

morphology have on the bleach-induced production and clearance of retinol. Additionally we wished to determine if there is a correlation between metarhodopsin decay rate (retinal release) and retinol production rate in different cell types. Due to the time-dependent wave-like spread of fluorescence that we observed in all cells, we confined the quantitative analysis of fluorescence kinetics in the outer segment to proximal regions of approximately similar longitudinal size: 1/4 of the OS of red rods was used and the whole OS of the cones and the green rods for this comparison.

The results of the analysis of fluorescence data are presented in Fig. 5 (A and B). Average data from red rods (black symbols) and red-sensitive cones (red

symbols) are plotted in Fig. 5 A; average data comparing the kinetics of green rods (green symbols) and blue-sensitive cones (blue symbols) are presented in Fig. 5 B. Metarhodopsin decay rates (retinal release) in red rods, green rods, and red-sensitive cones as assessed by MSP recordings are shown for comparison in Fig. 5 C.

We characterized the time course of retinol fluorescence changes by bi-exponential fits to the experimental data, of the form

$$I(t) = a \cdot (\exp(-t/\tau_2) - \exp(-t/\tau_1)), \qquad (4)$$

where $I(t)$ is the relative fluorescence intensity, a is a constant (>0), t is time, and τ_1 and τ_2 are time constants for the rising and decaying phase of retinol fluorescence. Since microfluorometry has no intrinsic standard that would allow the conversion of the measured fluorescence emission intensities into retinol concentrations, before fitting we scaled the retinol data as assessed by microfluorometry to best fit the retinol data as assessed by microspectrophotometry, as shown in Figs. 3 and 4.

It should be noted that while τ_2 obviously represents the time constant of retinol clearance from the outer segment, τ_1 has no strict mechanistic meaning. This is because retinol generation is a two-step process, involving retinal release from metaproducts and its subsequent reduction to retinol. Thus, it cannot generally be characterized by a single rate/time constant. However, the initial slope of the fitted curve, $a \cdot (1/\tau_1 - 1/\tau_2)(s^{-1})$, can be used as a phenomenological estimate of the rate of retinol production that would allow comparison across the cells. Since fluorescence data was scaled to MSP data prior to fitting by Eq. 4, the estimated initial slopes are directly proportional to the initial changes of the retinol concentration (normalized relative to the dark pigment) following the bleach. Time constants for the bi-exponential fits to retinol data are listed in Table I, and the time constants of metarhodopsin decay as well as the retinol production rates estimated from initial slopes are tabulated in Table II.

The main panel of Fig. 5 A shows a comparison between retinol production and clearance in salamander red rods (containing RH1) and red-sensitive cones (containing M/LWS). According to this analysis, the retinol production rate is 38 times faster in red-sensitive cones compared with the rate at the base of red rod outer segment (see Table II). Further, the clearance of retinol is ~26 times faster in salamander red-sensitive cones where the pigment is contained in plasma membrane compared with red-sensitive rod photoreceptors where the pigment is contained in OS discs. The inset in Fig. 5 A shows these fluorescence data plotted on an extended time scale to better demonstrate the large difference in the time course of retinol clearance.
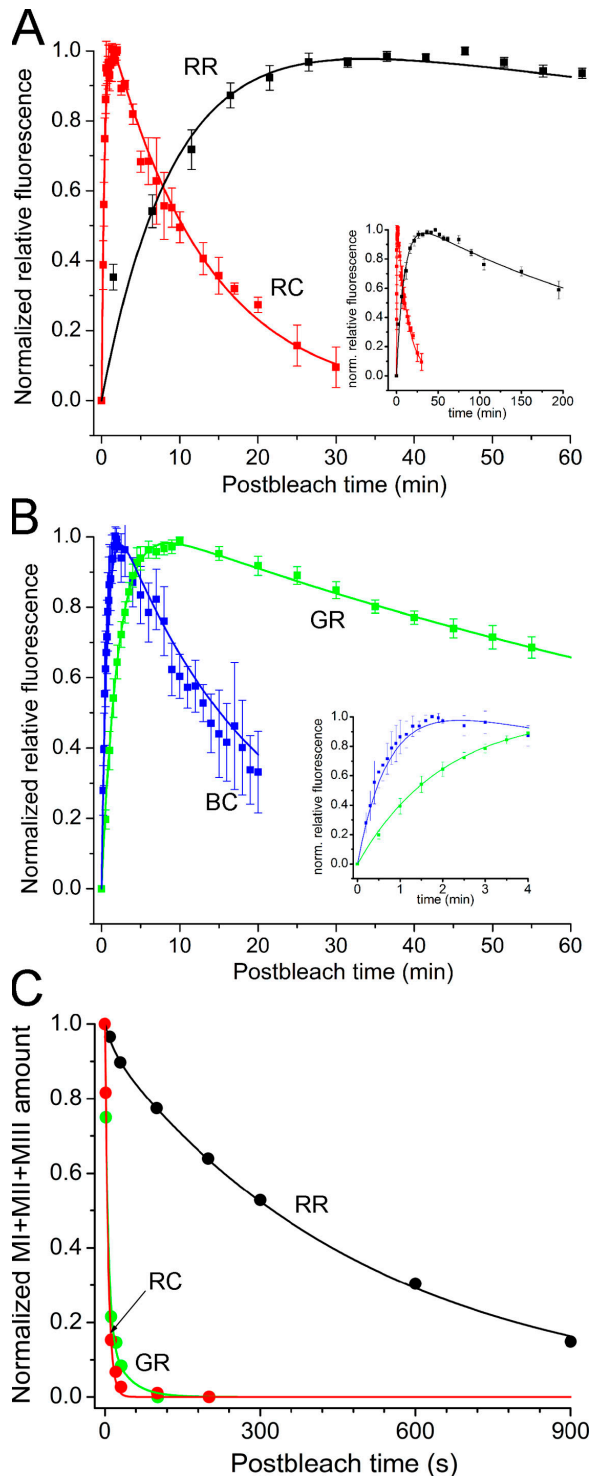
Ala-Laurila et al. 161

The data illustrated in Fig. 5 B show comparisons of the average rates of retinol production and its clearance in green rods and blue-sensitive cones. These two cell types share the same SWS2 visual pigment (Ma et al., 2001). In blue-sensitive cones, this pigment is embedded in the plasma membrane; in green rods, it is contained in internal discs. The inset shows these data plotted on an expanded time scale. Production of retinol occurs about threefold faster, and the clearance is about sevenfold faster in blue-sensitive cones than in green rods. These data show that retinol production rate is defined not only by the visual pigment type but also by other factors related to the RDH reaction as well.

The plots in Fig. 5 C show the metarhodopsin decay rates in salamander red rods, green rods, and red-sensitive cones measured by microspectrophotometry. It can be seen that there are substantial differences in the metaproduct decay rates among different photoreceptor cell types: metarhodopsin decay was significantly faster in both red-sensitive cones and green rods both containing cone-type pigments (M/LWS and SWS2, respectively) compared with red rods, which contain rod pigment (RH1). Thus, there is a crude correlation between the rate of decay of metaproducts and retinol production measured at the base of outer segments. According to both parameters, the cells can be arranged in the same rate-decreasing order: RC > GR > RR. This is not surprising since the rapid hydrolysis of the Schiff base in metarhodopsin(s) is expected to release all-trans retinal sooner, thus making it available to the RDH reaction earlier. However, the differences between metarhodopsin decay rates measured in the different cell types were much greater than were the respective differences in retinol production rates. For example, metapigment decay rate was >70 times faster in red-sensitive cones compared with red rods, whereas the rate of retinol production was only 38 times faster in red-sensitive cones compared with the retinol production rate at the basal OS of red rods. Similarly, metapigment decay proceeded identically at the tip and base of the OS; however the rates of retinol production at the two locations were grossly different (Figs. 1, 3, and 4). A simple mathematical model that quantifies the contributions of these two reactions in different photoreceptor

Figure 5. Comparisons of the time course of retinol fluorescence changes measured in different salamander rod and cone outer segments after bleaching the visual pigment. In all cases, >90% of pigment was bleached by a step of light at time = 0. (A) Comparison of the time course of average post-bleach fluorescence production and clearance (mean ± SEM) of red-sensitive cones (RC, red squares, $n = 4$) and red rods (RR, black squares, $n = 7$). The inset in A compares the time course of retinol fluorescence changes over a longer time period to demonstrate the differences in the clearance rates of retinol between rod- and cone-type photoreceptors. (B) Comparison of the kinetics of fluorescence pro-

duction in salamander blue-sensitive cones (BC, blue squares, $n = 3$) and green rods (GR, green squares, $n = 5$), which contain identical visual pigments (mean ± SEM). Inset in B compares the difference in the kinetics of the rising phase of fluorescence of blue-sensitive cones and green rods. Continuous curves in A and B are fitted to the data according to Eq. 4. The time constants (τ_1, τ_2) of the best-fitting bi-exponential models shown in A and B are listed in Table I. (C) Comparison of the rates of metaproduct decay (=retinal production) in various types of photoreceptors. The data are fitted with either single-exponential (RC) or bi-exponential function (RR and GR). Parameters of the fits are given in Table II.

TABLE I

Time course of Production and Clearance of Retinol Fluorescence As Assessed by Microfluorometry in Salamander Red Rods (RR), Green Rods (GR), Red-sensitive Cones (RC), and Blue-sensitive Cones (BC)

	OS dimensions											Two-exponential fit to ROL fluorescence, normal Ringer					Two-exponential fit to ROL fluorescence, IRBP (100 μM)				
	L		d		V		S		S/V		τ_1		τ_2			τ_1		τ_2		
	μm		μm		μm³		μm²		μm⁻¹		min		min			min		min		
Cell type	Mean	SEM	Mean	SEM	Mean	SEM	Mean	SEM	Mean	SEM	Mean	SEM	Mean	SEM	n	Mean	SEM	Mean	SEM	n
Red rod (RR)	27	0.8	10	0.2	2260	92	941	28	0.42	0.01	9.22	0.94	324	56	7	8.50	–	25.0	–	6
Green rod (GR)	14	1.3	8.2	0.4	731	78	403	33	0.57	0.02	2.07	0.26	123	13	5	–	–	–	–	
Red-sensitive cone (RC)	7.8	0.5	3.3	0.1	70	19	88.1	19	1.28	0.1	0.39	0.08	12.5	2.4	4	0.28	0.04	4.0	0.9	6
Blue-sensitive cone (BC)	7.8	0.8	3.2	0.1	61.6	2.6	83.2	5	1.35	0.03	0.72	0.24	17.9	6.0	3	–	–	–	–	

Photoreceptor dimensions (mean ± SEM) and the time constants for the production and clearance of retinol fluorescence are shown for each of the photoreceptor types studied. Mean estimates for photoreceptor dimensions were obtained as explained in Materials and Methods using the bright field images of cells obtained during fluorescence recordings. Mean estimates for the time constants of production and clearance of retinol fluorescence are obtained by fitting fluorescence data from each individual cell using a bi-exponential function (see Eq. 4, Results). In order to facilitate interphotoreceptor comparisons, these fits were carried out using OS regions of comparative longitudinal size: the most proximal 1/4 of the OSs in RR and the whole OSs of GR, BC, and RC. *L*, the length of the OS; *d*, mean diameter of the OS; *V*, estimated OS volume (see Materials and Methods); *S*, estimated total surface area of the OS without invaginations (see Materials and Methods); *S/V*, surface to volume ratio of the cell; τ_1, time constant for the rising phase of retinol fluorescence (see text for discussion about the strict mechanistic meaning); τ_2, time constant for the falling phase of retinol fluorescence = time constant for retinol clearance; *n*, number of cells comprising the average.

types and different regions of their outer segments is presented in Discussion.

Effect of IRBP on Retinol Clearance

Mechanisms of retinol transfer from the outer segments to further processing steps are poorly understood. Both fluorometric and MSP measurements performed in standard Ringer solution demonstrated that, after its production, retinol is translocated from the outer segment (Figs. 4 and 5). However, it has been shown earlier by Tsina et al. (2004) in bleached salamander red rods that when no lipophilic substance is present in the bathing solution, retinol fluorescence declines slowly and may persist for hours. Furthermore, this study showed that the clearance of retinol was significantly accelerated in salamander red rods in the presence of exogenous lipophilic substances (IRBP and BSA; IRBP being substantially more efficient than BSA). Thus, we performed experiments to assess whether the clearance of retinol can be facilitated by IRBP, and to determine if the rate of production of retinol and its clearance from the cell are essentially independent of one another. IRBP, a 140-kD glycoprotein (Shaw and Noy, 2001; Loew and Gonzalez-Fernandez, 2002), is the most abundant soluble protein in the interphotoreceptor matrix. It has been shown to bind retinoids and is believed to assist in the transfer of retinol from photoreceptors to the retinal pigment epithelium and/or to Müller cells (Edwards and Adler, 2000; Tsina et al., 2004; Qtaishat et al., 2005). Fig. 6 illustrates the time course of fluorescence changes that occur following bright light in the absence and presence of 100 μM IRBP added to the superfusate.

Measurements were made on salamander red rods and red-sensitive cones as examples of the two different cell morphologies (pigment enclosed in discs vs. pigment embedded in the plasma membrane). The continuous curves through the data points were constructed as bi-exponential fits to the experimental data according to Eq. 4. As can be seen from the data presented in Fig. 6 and from the time constants of retinol clearance (τ_2) shown in Table I, IRBP treatment resulted in an increase of >10-fold in the rate of clearance of retinol from red rods and about a threefold increase in the rate in red-sensitive cones. In addition, the peak level of fluorescence measured in the presence of IRBP in both cell types was significantly lower than when no IRBP was present (unpublished data). These changes in the peak levels of fluorescence were consistent with the observed acceleration of the clearance rate.

The Dependence of Retinol Clearance on the Surface to Volume Ratio of the Photoreceptor

We have shown by fluorescence measurements and microspectrophotometry that clearance of retinol from salamander cones occurs 18–26-fold faster than from salamander red rods (see Fig. 5; Table I). This finding is generally consistent with a faster operation of the cone visual cycle. As clearance implies the transfer of retinol across the OS plasma membrane to its outer face, photoreceptors with the largest surface to volume ratios may be expected to have higher clearance rates of retinol. A test of this notion is shown in Fig. 7.

Here the mean estimates of the rate constants of retinol clearance ($1/\tau_2$) are plotted against the average surface to volume ratio for each cell type. Both axes are plotted on logarithmic scale. The surface to volume ratio estimates were calculated as described in Materials and Methods without taking into account the invaginations

TABLE II
Time Constants of Metaproduct Decay and Rates of Retinal-to-Retinol Conversion in Various Cell Types

Parameter	a_1	τ_{m1}, s	a_2	τ_{m2}, s	k_1, s^{-1}	k_2/k_1	ROL production rate, s^{-1}
Base						0.95	1.0×10^{-3}
RR	0.06	20	0.94	514	0.0021		
Tip						0.58	5.3×10^{-4}
Base						0.25	
GR	0.81	6.2	0.19	35	0.11		4.8×10^{-3}
Tip						0.19	
RC	1	6.7	0	–	0.15	0.31	3.8×10^{-2}
BC	NA	NA	NA	NA	NA	NA	1.4×10^{-2}

a_1, a_2 and τ_{m1}, τ_{m2} are amplitudes and time constants of the bi-exponential fits to the decay of metaproducts (meta I+II+III). k_1 is the first-order rate constant of retinal release from metarhodopsins obtained from a single-exponential fit of the metaproducts' curve. k_2 is the rate constant of retinal-to-retinol conversion; values of k_2/k_1 in the last column are taken from Fig. 8. Retinol production rates were estimated from fluorescence data as a·$(1/\tau_1 - 1/\tau_2)$, where a, τ_1, and τ_2 are parameters of a bi-exponential fit to the fluorescence curve scaled accordingly to the MSP data (see in the main text). NA, not available.

in the OS membranes. Black symbols correspond to relative clearance rates measured in Ringer solution (from left to right: red rods, green rods, red-sensitive cones, and blue-sensitive cones). Green symbols correspond to the clearance rates measured in the presence of 100 μM IRBP. Straight lines through the experimental points correspond to power functions; the dashed line shows a linear relation on log-log coordinates. It is obvious from the comparison between the data and the dashed line that the clearance rate increases more steeply than would be predicted by assuming a linear relation between the clearance rate and the surface to volume ratio (without invaginations). Thus, it appears that cone invaginations increase the effective surface to volume ratio for retinol clearance, although this effect is not as large as would be expected from purely geometric considerations. If cone outer segment membrane invaginations are considered (assuming ∼33 discs/μm of OS length; Blaurock and Wilkins, 1969; Vanderkooi and Sundaralingam, 1970), a 50-fold larger surface to volume ratio is calculated (unpublished data). However, the prediction based on the rod data and the clearance rate in cones is that the invaginations only increase the effective surface to volume ratio by a factor of two to three. This modest effect may be due to the limited diffusional accessibility of the extracellular spaces between adjacent infoldings of the plasma membrane.

DISCUSSION

We have characterized the rates of the principal reactions of the visual cycle that occur within intact isolated salamander photoreceptors after bleaching. These sequential key reactions are the hydrolysis of the Schiff base linkage in metarhodopsins that liberates all-trans retinal, the reduction of all-trans retinal to all-trans retinol, and the translocation of all-trans retinol from the outer segment to the extracellular matrix before its uptake by the retinal pigment epithelium or Müller cells. The cell types that we investigated included salamander rod and cone photoreceptors: red rods with the rod pigment (RH1), green rods with the cone pigment (SWS2), as well as blue- and red-sensitive cones with the cone pigments (SWS2 and M/LWS, respectively).

Comparison of Retinol Kinetics As Obtained by Microfluorometry and Microspectrophotometry

An important consideration in the analysis and interpretation of our data is whether the observed fluorescence changes truly represent the entire pool of retinal found in salamander photoreceptors and whether fluorescence and microspectrophotometry data are in agreement. The former question arises from the fact that salamander photoreceptor cells contain a mixture of vitamin A1 and A2 chromophores. It has been shown earlier that the fluorescence signal comes mostly from retinol (A1) because the quantum yield of its fluorescence is almost 40-fold higher than that of dehydroretinol (A2) (Tsin et al., 1988). The latter question arises because absorbance measurements made with the MSP allow characterization of the total chromophore composition in each cell and yield total concentration of both forms of retinol (see Materials and Methods).

As MSP has shown, different animals may have greatly varying proportions of A1/A2 chromophores. However, no significant differences in time courses of photoproducts were found between the cells of the same type with the A1/A2 ratio differing in the range of 20%/80%–75%/25%. Nevertheless, fitting the absorbance spectra with a mixture of A1/A2 retinal and retinol templates revealed that the final products at the end of photolysis in both types of rods clearly contained a lower proportion of dehydroretinal and higher proportion of dehydroretinol compared with the dark pigment. The result may indicate
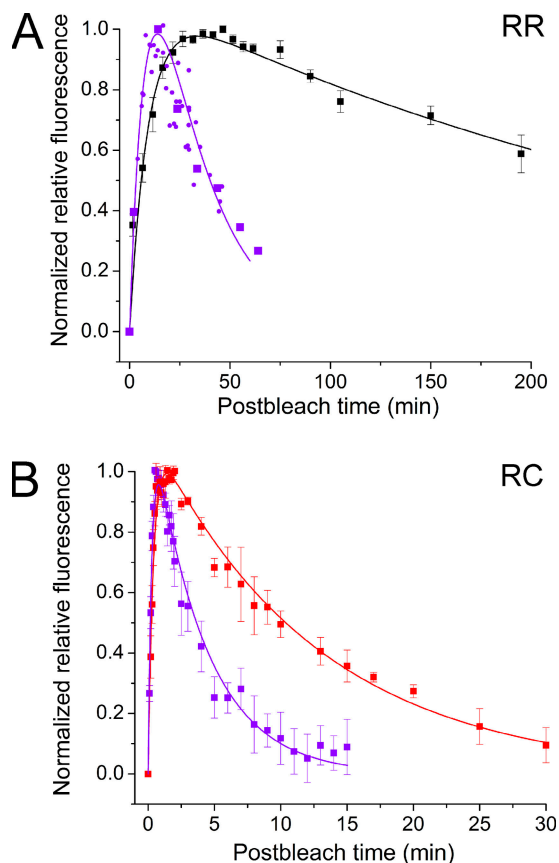
Figure 6. The effect of presence and absence of 100 µm IRBP on post-bleach production and clearance of retinol in rod and cone outer segments. (A) Comparison of time course of fluorescence changes in salamander red rod OSs in normal Ringer (RR, black squares, $n = 7$) and in the presence of IRBP (violet symbols). Small violet circles comprise recordings from a single cell; violet squares represent average data ($n = 5$, replotted from Tsina et al. 2004). (B) Comparison of the time course of normalized average fluorescence in salamander red-sensitive cone OSs in normal Ringer (RC, red squares, $n = 4$) and in the presence of IRBP (violet squares, $n = 6$). Continuous lines are fitted according to Eq. 4. (See Table I for the time constants). Error bars: SEM.

that dehydroretinal (A2) is a preferred substrate for RDH, and retinol (A1) is more readily cleared from the rods. This may explain the difference between the retinol/dehydroretinol time courses in rods as assessed by MSP and microfluorometry (Fig. 3 C; Fig. 4 A). Remarkably, the discrepancy is not seen in red-sensitive cones that contained not more than 10% of A2- chromophore (Fig. 4 B).

Obviously, the problem of specificity of retinol production and clearance needs further investigation. However, reasonable-to-good agreement between the results obtained by fluorometry and MSP shows that the mixed chromophore composition does not critically compromise our analysis.

Decay of Metaproducts

The hydrolysis of the Schiff base linkage between all-trans retinal and opsin renders the chromophore-binding
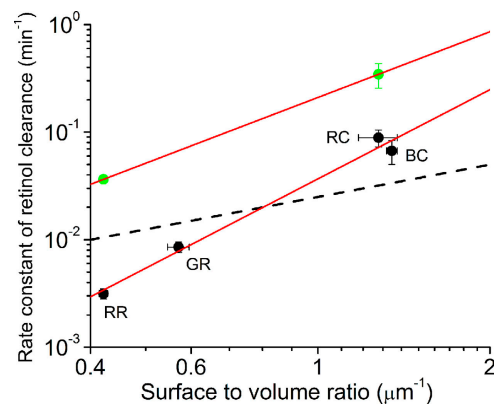

Figure 7. The dependence of the relative rates of retinol clearance on the surface to volume ratio of rod and cone photoreceptor outer segments. The clearance rate of retinol (mean ± SEM) of each cell type is plotted against the mean estimate of surface to volume ratio of each photoreceptor type (numerical values shown in Table I). The data are plotted on logarithmic scale. Black symbols correspond to measurements in normal Ringer (from left to right): salamander red rods (RR, $n = 7$), salamander green rods (GR, $n = 5$), salamander red-sensitive cones (RC, $n = 4$), and salamander blue-sensitive cones (BC, $n = 3$). Green symbols correspond to measurements in the presence of IRBP (100 µM) (from left to right): salamander red rods ($n = 6$) and salamander red-sensitive cones ($n = 6$). The red continuous lines show the best-fitting power functions to measurements in Ringer and in the presence of IRBP. Dashed black line shows the best fitting line that assumes linear dependence between the clearance rate and the S/V ratio.

site on opsin vacant and available for recombination with 11-cis retinal that results in the regeneration of the dark visual pigment. It is probable that this is the step that sets the speed of dark adaptation at low bleaching levels, provided that there is a preexisting store of 11-cis chromophore available to the photoreceptors. This idea is supported by findings that rods in isolated retina can regenerate up to 10% rhodopsin without contact with the RPE (Donner and Hemilä, 1975; Azuma et al., 1977; Cocozza and Ostroy, 1987).

Besides providing free opsin for the restoration of the dark pigment, the decay of metaproducts plays another important role in quenching the phototransduction cascade after moderate bleaches. Phosphorylated and arrestin-bound metarhodopsins generate a background signal whose cessation is necessary for complete restoration of retinal sensitivity (Leibrock et al., 1994, 1998). At high bleaches, the signaling activity of metarhodopsins keeps the receptor in saturation, making it functionally insensitive to light (Firsov et al., 2005). Therefore, irrespective of the regeneration of dark pigment, the decay of metaproducts is necessary for recovery of photoreceptor sensitivity.

The much more rapid rate of dark adaptation of cone vision as compared with rod vision implies correspondingly faster photoproduct decay of cone visual pigments compared with rod pigments. Our results demonstrate that it is indeed the case. Fig. 5 C summarizes the results

Ala-Laurila et al.   165

obtained by microspectrophotometry. As an extreme example, the time constant of metaproduct decay in salamander red-sensitive cones is ~70 times shorter than in salamander red rods (6.7 vs. 470 s, respectively). Green rods occupy an intermediate position (Fig. 5 C; see also Golobokova et al., 2003). This is in agreement with the results recently obtained by Golobokova and Govardovskii (2006) on goldfish rods and cones. Thus, the prerequisite condition of faster metaproduct decay for faster dark adaptation of cones compared with rods is fulfilled.

The Rate-limiting Step of Retinol Production

Both fluorescent imaging and microspectrophotometry show that the rate of retinol production after bleaching is highly nonuniform, both among different cell types and different locations within the photoreceptor outer segment. As for different cell types, the rate of retinol generation was significantly faster in all cells (red- and blue-sensitive cones and green rods) containing cone pigments (M/LWS and SWS2) as compared with red rods with the rod pigment (RH1). Also, in all types of cells studied, the fastest rates of retinol generation were observed at the bases of the outer segments, and the slowest, at the tips (Figs. 1–4, see also Tsina et al., 2004). Notably, the rate of retinol production can be different in the cells sharing the same pigment (salamander green rods vs. blue cones, Fig. 5 B). Also, there is no regional difference in metaproduct decay within the same cell (Fig. 3). Thus it is obvious that retinol generation depends not only on the availability of the substrate (all-trans retinal), but also on the rate of its reduction by RDH.

A rigorous theoretical treatment of retinal to retinol reduction is not possible because of lack of data on the RDH kinetic parameters and concentrations of cofactors (NADP and NADPH) in intact cells. However, rates of retinal production and reduction can be semi-quantitatively compared within the framework of a simple kinetic model. Let us assume that metaproducts decay along a single exponent, $M(t) = \exp(-k_1 \cdot t)$, which is a good approximation for each cell type we studied. Further assume that the RAL to ROL conversion can be described by a Michaelis-like kinetics with the maximum rate k_2 (s^{-1}) and apparent Michaelis constant $K_M << 1$ (Palczewski et al., 1994; notice that K_M is dimensionless and expressed as a fraction of bleached visual pigment). Also assume that the ROL clearance follows first-order kinetics with the rate constant k_3. Then, by solving appropriate differential equations, one can find concentrations of RAL and ROL as shown in the inset of Fig. 8.

The relative peak concentration of RAL (with respect to the bleached pigment) is a function of the k_2/k_1 ratio and thus can be used to characterize the speed of RAL to ROL conversion. The advantage of using RAL rather than ROL is that its concentration, in contrast to the latter, is not affected by ROL removal from the OS. The red curve in the main panel of Fig. 8 shows the prediction of the model, and dots on the curve show peak RAL concentrations obtained from the MSP measurements in various cell types and locations. The part of the graph to the left of the vertical dashed line corresponds to $k_2 < k_1$, that is, to the situation when the generation of ROL is limited by the RDH reaction. Conversely, the points to the right correspond to the limitation by the metarhodopsin decay. It is seen that at the RR base, the rate of retinal release from metarhodopsins is approximately equal to the rate of its reduction by RDH. At the RR tip, the reduction is twofold slower than the decay, and in all other cases, retinal is released substantially faster than it can be reduced to retinol.

We hypothesize that the regional differences in the rate of retinol production within the same cell arise from the limited supply of the RDH cofactor NADPH rather than from different properties of the RDH enzyme itself. The wave-like spread of retinol fluorescence within the OS is consistent with the idea that retinol generation is dependent on a substrate that is delivered from the inner segment (Fig. 1; see also Tsina et al., 2004). The idea is also supported by the existence of the regional difference in cones where diffusional shuffling of membrane components in the continuous OS structure should make the RDH properties uniform over the OS length.

NADPH is necessary for reduction of retinal to retinol by RDH (Futterman, 1963). Its amount in dark-adapted photoreceptor outer segment cannot be sufficient for complete reduction of retinal to retinol after a near-100% bleach. Such a high concentration (~3 mM) would result in a significant (and probably varying) increase in the absorbance at ~340 nm in the region of the spectrum near the rhodopsin β-band. Such increased absorbance has never been observed in MSP measurements. Hence, we assume that the initial fast stage of retinol production may rely on a small preexisting pool of NADPH within the outer segments that may comprise ~10% of the dark pigment (as inferred from the magnitude of the initial fast retinol increase seen in fluorescence measurements, Fig. 5). After the pool is exhausted, the rate of retinol production is limited by the rate of NADPH supply (Tsina et al., 2004).

The production of NADPH in the OS is not yet completely understood in quantitative terms. It has been shown that rod outer segments contain both the glucose transporter and the biochemical reactions for the anaerobic utilization of glucose (Hsu and Molday, 1991), including the hexose monophosphate pathway that produces NADPH. The rate of NADPH production in bovine rod outer segment preparations in optimal condition is 40 nmol/min/mg ROS protein (Hsu and Molday, 1994). The fastest retinol production that we observed in salamander red-sensitive cones was

0.038 s^{-1} = 2.3 min^{-1} (Table II). Since the number is normalized to bleached visual pigment, and there is ~12 nmol rhodopsin per milligram ROS protein, it translates into consumption of ~30 nmol NADPH/min/mg ROS protein. Thus, the rate of NADPH generation measured by Hsu and Molday (1994) seems more than sufficient to support the fastest retinal-to-retinol conversion. However, it is not clear whether the data obtained in vitro can be applied to the situation in intact outer segments. The wave-like development of fluorescence observed in our experiments (see also Tsina et al., 2004) is more in line with the notion that after exhaustion of the local store, retinal reduction relies mostly on the NADPH that derives from energy supplies (ATP, phosphocreatine, malate, etc.) that are produced in the inner segment/ellipsoid regions of the cells. Additional sources of NADPH could derive from NADP$^+$-linked dehydrogenases or NADH/NADPH transhydrogenases that operate in these regions (Tsina et al., 2004; Chen et al., 2005). It may also be that the NADPH supply is the factor that limits the speed of the RDH reaction in cones where its substrate, retinal, is generated quickly from decaying metaproducts. Clearly, a quantitative study of NADPH production in intact photoreceptors is necessary to clarify this issue.

It has been hypothesized that in addition to providing the substrate for making 11-cis retinal via RPE and/or Müller cells, reduction of retinal to retinol plays other important roles in photoreceptor function. For instance, it may serve to remove potentially toxic retinal by converting it to more benign retinol. Failure to eliminate retinal due to a defective RDH pathway is implicated in the genesis of Stargardt's disease (Rattner et al., 2000). Besides being toxic, all-trans retinal and all-trans retinol have both been shown to block cGMP-gated cationic channels of the OS plasma membrane (Dean et al., 2002; McCabe et al., 2004; Horrigan et al., 2005). Thus, the reduction of retinal to retinol and its subsequent translocation from the OS may be necessary for complete recovery of photoreceptor dark current. The latter problem may be especially acute in cones that function at high intensities (hence higher levels of bleaching). In accordance with this, we find that the maximum rate of retinol production in salamander cones is 38-fold higher than the maximum rate in red rods (Table II).

Retinol Clearance

The last step of the visual cycle within the photoreceptor outer segment is the transfer of all-trans retinol through the plasma membrane to the extracellular space. This step serves both as the source of substrate for the reactions of the visual cycle in RPE and Müller cells, and also as a means of clearance of retinol from the OS to facilitate the recovery of the dark current. The rate of unaided clearance of retinol inferred from
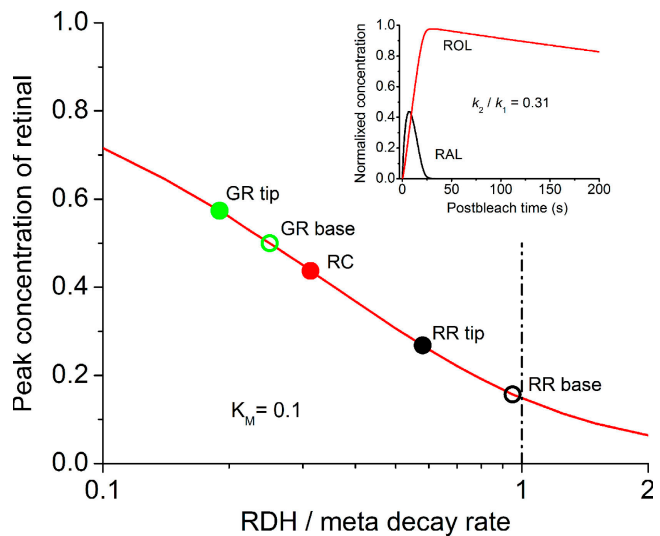

Figure 8. Assessing relative rates of retinal and retinol generation from the height of the retinal peak. The red curve in the main panel shows the peak retinal concentration as a function of k_2/k_1 ratio calculated based on the model described in the text and assuming $K_M = 0.1$. Dots correspond to peak retinal concentrations obtained by the MSP for various cell types. Inset, an example of RAL and ROL time courses calculated for the RAL peak 0.44 and $k_1 = 0.15$ s^{-1}, as measured with MSP in RC. Height of the RAL peak corresponds to the k_2/k_1 ratio of 0.31.

our experiments is too slow compared with the regeneration rate of the visual pigment. Normally, rhodopsin regeneration is virtually complete within ~1 h while the time constant of retinol clearance from red rods in standard Ringer solution is roughly 5 h (Table I). Similarly, a 12–18-min time constant for retinol removal from cones (Table I) would imply ~30 min for complete recycling of cone chromophore, provided that delays at other stages of the cycle can be neglected.

The foregoing considerations suggest that there are additional mechanisms that must facilitate retinol clearance from the outer segment and its transfer to further processing steps. One candidate agent is IRBP. Its role as a chaperon to traffic retinoids between photoreceptors and RPE cells has long been discussed (for recent review see Lamb and Pugh, 2004). Its key importance, however, has been questioned based on results with IRBP-knockout mice whose visual cycle appeared only modestly perturbed (Palczewski et al., 1999; Ripps et al., 2000). We have shown here that the presence of IRBP in the bathing solution greatly accelerates retinol clearance from all photoreceptor types studied, so it becomes more compatible with the overall rate of the visual cycle. Still, transfer of retinol from the OS to the intercellular space remains the slowest step of the visual cycle within photoreceptors.

The fact that all-trans retinal in isolated photoreceptors can be virtually completely converted to retinol, and a substantial fraction of the latter can be cleared to

the extracellular space (Fig. 1 B and Figs. 2 and 3), is at variance with the so-called tunneling hypothesis. This hypothesis suggests that all-trans retinal released from the chromophore binding site after bleaching stays bound at an exit site of opsin and can only be removed from it when "fresh" 11-cis retinal binds to an entrance site before regeneration can occur (Heck et al., 2003; Schädel et al., 2003). If the proposed tunneling mechanism were obligatory, it would mean that no all-trans retinoid generated after bleach could be removed from the OS without first providing 11-cis retinal. This is clearly not the case in our experiments done on isolated cells devoid of any 11-cis retinal supply.

Taken together, the results we present here provide a mechanistic basis for the much more rapid operation of the visual cycle in cone photoreceptors compared with rod photoreceptors. This is so for three principal reasons. First, metapigment decay occurs much more rapidly in cells containing cone pigment compared with cells containing rod pigment. Second, the reduction of retinal to retinol occurs more rapidly in cones than in rods. Third, retinol clearance is significantly faster from cones than from rods because of the larger surface to volume ratio of cones. The first two reasons, i.e., fast metarhodopsin decay rate as well as the fast RDH reaction in cones, also underlie the faster retinol production rates observed in cones compared with rods. In rods containing rod-type pigment, the metapigment decay rate is significantly slower than in cells containing cone-type pigments, and in certain regions of the outer segment (i.e., the distal tip), retinol production appears to be limited by factors unrelated to metapigment decay. We hypothesize that this limitation is likely due to insufficient supplies of the RDH cofactor, NADPH, that derive from energy sources within mitochondria located in the inner segments of these cells. Additional comparative studies of the energy metabolism of rods and cones will be required to determine the dynamic role of NADPH production in the operation of the visual cycle to resolve this issue.

Olaf S. Andersen served as editor.

REFERENCES

Azuma, K., M. Azuma, and W. Sickel. 1977. Regeneration of rhodopsin in frog outer segments. *J. Physiol.* 271:747–759.

Baylor, D.A., T.D. Lamb, and K.W. Yau. 1979. The membrane current of single rod outer segments. *J. Physiol.* 288:589–611.

Blaurock, A.E., and M.H. Wilkins. 1969. Structure of frog photoreceptor membranes. *Nature.* 223:906–909.

Chen, C., E. Tsina, M.C. Cornwall, R.K. Crouch, S. Vijayaraghavan, and Y. Koutalos. 2005. Reduction of all-trans retinal to all-trans retinol in the outer segments of frog and mouse rod photoreceptors. *Biophys. J.* 88:2278–2287.

Cocozza, J.D., and S.E. Ostroy. 1987. Factors affecting the regeneration of rhodopsin in the isolated amphibian retina. *Vision Res.* 27:1085–1091.

Cohen, G.B., D.D. Oprian, and P.R. Robinson. 1992. Mechanism of activation and inactivation of opsin: role of Glu113 and Lys296. *Biochemistry.* 31:12592–12601.

Cornwall, M.C., E.F. MacNichol Jr., and A. Fein. 1984. Absorptance and spectral sensitivity measurements of rod photoreceptors of the tiger salamander, *Ambystoma tigrinum. Vision Res.* 24:1651–1659.

Cornwall, M.C., A. Fein, and E.F. MacNichol Jr. 1990. Cellular mechanisms that underlie bleaching and background adaptation. *J. Gen. Physiol.* 96:345–372.

Cornwall, M.C., G.J. Jones, V.J. Kefalov, G.L. Fain, and H.R. Matthews. 2000. Electrophysiological methods for measurement of activation of phototransduction by bleached visual pigment in salamander photoreceptors. *Methods Enzymol.* 316:224–252.

Das, S.R., N. Bhardwaj, H. Kjeldbye, and P. Gouras. 1992. Muller cells of chicken retina synthesize 11-cis-retinol. *Biochem. J.* 285(Pt 3):907–913.

Dean, D.M., W. Nguitragool, A. Miri, S.L. McCabe, and A.L. Zimmerman. 2002. All-trans-retinal shuts down rod cyclic nucleotide-gated ion channels: a novel role for photoreceptor retinoids in the response to bright light? *Proc. Natl. Acad. Sci. USA.* 99:8372–8377.

Donner, K.O., and S. Hemilä. 1975. Kinetics of long-lived rhodopsin photoproducts in the frog retina as a function of the amount bleached. *Vision Res.* 15:985–995.

Ebrey, T., and Y. Koutalos. 2001. Vertebrate photoreceptors. *Prog. Retin. Eye Res.* 20:49–94.

Edwards, R.B., and A.J. Adler. 2000. IRBP enhances removal of 11-cis-retinaldehyde from isolated RPE membranes. *Exp. Eye Res.* 70:235–245.

Firsov, M.L., A.V. Kolesnikov, E.Y. Golobokova, and V.I. Govardovskii. 2005. Two realms of dark adaptation. *Vision Res.* 45:147–151.

Fukada, Y., and T. Yoshizawa. 1981. Activation of phosphodiesterase in frog rod outer segment by an intermediate of rhodopsin photolysis. II. *Biochim. Biophys. Acta.* 675:195–200.

Futterman, S. 1963. Metabolism of the retina. *J. Biol. Chem.* 238:1145–1150.

Golobokova, E.Y., and V.I. Govardovskii. 2006. Late stages of visual pigment photolysis in situ: cones vs. rods. *Vision Res.* 46:2287–2297.

Golobokova, E.Y., A.V. Kolesnikov, and V.I. Govardovskii. 2003. Slow stages of photolysis of the green rods visual pigment of the frog, *Rana temporaria. Sens. Syst.* 17:134–143 (in Russian).

Govardovskii, V.I., and L.V. Zueva. 2000. Fast microspectrophotometer for studying the photolysis of visual pigments *in situ. Sensornye Sistemy.* 14:288–296.

Govardovskii, V.I., N. Fyhrquist, T. Reuter, D.G. Kuzmin, and K. Donner. 2000. In search of the visual pigment template. *Vis. Neurosci.* 17:509–528.

Hárosi, F.I. 1975. Absorption spectra and linear dichroism of some amphibian photoreceptors. *J. Gen. Physiol.* 66:357–382.

Heck, M., S.A. Schädel, D. Maretzki, and K.P. Hofmann. 2003. Secondary binding sites of retinoids in opsin: characterization and role in regeneration. *Vision Res.* 43:3003–3010.

Horrigan, D.M., M.L. Tetreault, N. Tsomaia, C. Vasileiou, B. Borhan, D.F. Mierke, R.K. Crouch, and A.L. Zimmerman. 2005. Defining the retinoid binding site in the rod cyclic nucleotide-gated channel. *J. Gen. Physiol.* 126:453–460.

Hsu, S.C., and R.S. Molday. 1991. Glycolytic enzymes and a GLUT-1 glucose transporter in the outer segments of rod and cone photoreceptor cells. *J. Biol. Chem.* 266:21745–21752.

Hsu, S.C., and R.S. Molday. 1994. Glucose metabolism in photoreceptor outer segments. Its role in phototransduction and in NADPH-requiring reactions. *J. Biol. Chem.* 269:17954–17959.

Jäger, S., K. Palczewski, and K.P. Hofmann. 1996. Opsin/all-trans-retinal complex activates transducin by different mechanisms than photolyzed rhodopsin. *Biochemistry.* 35:2901–2908.

Jones, G.J., R.K. Crouch, B. Wiggert, M.C. Cornwall, and G.J. Chader. 1989. Retinoid requirements for recovery of sensitivity after visual-pigment bleaching in isolated photoreceptors. *Proc. Natl. Acad. Sci. USA.* 86:9606–9610.

Jones, G.J., A. Fein, E.F. MacNichol Jr., and M.C. Cornwall. 1993. Visual pigment bleaching in isolated salamander retinal cones. Microspectrophotometry and light adaptation. *J. Gen. Physiol.* 102:483–502.

Kolesnikov, A.V., E.Y. Golobokova, and V.I. Govardovskii. 2003. The identity of metarhodopsin III. *Vis. Neurosci.* 20:249–265.

Lamb, T.D., and E.N. Pugh Jr. 2004. Dark adaptation and the retinoid cycle of vision. *Prog. Retin. Eye Res.* 23:307–380.

Leibrock, C.S., T. Reuter, and T.D. Lamb. 1994. Dark adaptation of toad rod photoreceptors following small bleaches. *Vision Res.* 34:2787–2800.

Leibrock, C.S., T. Reuter, and T.D. Lamb. 1998. Molecular basis of dark adaptation in rod photoreceptors. *Eye.* 12:511–520.

Liebman, P.A. 1969. Microspectrophotometry of retinal cells. *Ann. NY Acad. Sci.* 157:250–264.

Liebman, P.A. 1973. Microspectrophotometry of Visual Receptors. *In* Biochemistry and Physiology of Visual Pigments. H. Langer, editor. Springer-Verlag, New York. 299–305.

Loew, A., and F. Gonzalez-Fernandez. 2002. Crystal structure of the functional unit of interphotoreceptor retinoid binding protein. *Structure.* 10:43–49.

Ma, J., S. Znoiko, K.L. Othersen, J.C. Ryan, J. Das, T. Isayama, M. Kono, D.D. Oprian, D.W. Corson, M.C. Cornwall, et al. 2001. A visual pigment expressed in both rod and cone photoreceptors. *Neuron.* 32:451–461.

Mahroo, O.A., and T.D. Lamb. 2004. Recovery of the human photopic electroretinogram after bleaching exposures: estimation of pigment regeneration kinetics. *J. Physiol.* 554:417–437.

Makino, C.L., and R.L. Dodd. 1996. Multiple visual pigments in a photoreceptor of the salamander retina. *J. Gen. Physiol.* 108:27–34.

Mariani, A.P. 1986. Photoreceptors of the larval tiger salamander retina. *Proc. R. Soc. Lond. B. Biol. Sci.* 227:483–492.

Mata, N.L., R.A. Radu, R.C. Clemmons, and G.H. Travis. 2002. Isomerization and oxidation of vitamin a in cone-dominant retinas: a novel pathway for visual-pigment regeneration in daylight. *Neuron.* 36:69–80.

McBee, J.K., K. Palczewski, W. Baehr, and D.R. Pepperberg. 2001. Confronting complexity: the interlink of phototransduction and retinoid metabolism in the vertebrate retina. *Prog. Retin. Eye Res.* 20:469–529.

McCabe, S.L., D.M. Pelosi, M. Tetreault, A. Miri, W. Nguitragool, P. Kovithvathanaphong, R. Mahajan, and A.L. Zimmerman. 2004. All-trans-retinal is a closed-state inhibitor of rod cyclic nucleotide-gated ion channels. *J. Gen. Physiol.* 123:521–531.

Morton, R.A., and G.A. Pitt. 1955. Studies on rhodopsin. IX. pH and the hydrolysis of indicator yellow. *Biochem. J.* 59:128–134.

Palczewski, K., S. Jager, J. Buczylko, R.K. Crouch, D.L. Bredberg, K.P. Hofmann, M.A. Asson-Batres, and J.C. Saari. 1994. Rod outer segment retinol dehydrogenase: substrate specificity and role in phototransduction. *Biochemistry.* 33:13741–13750.

Palczewski, K., J.P. Van Hooser, G.G. Garwin, J. Chen, G.I. Liou, and J.C. Saari. 1999. Kinetics of visual pigment regeneration in excised mouse eyes and in mice with a targeted disruption of the gene encoding interphotoreceptor retinoid-binding protein or arrestin. *Biochemistry.* 38:12012–12019.

Pitt, G.A., F.D. Collins, R.A. Morton, and P. Stok. 1955. Studies on rhodopsin. VIII. Retinylidenemethylamine, an indicator yellow analogue. *Biochem. J.* 59:122–128.

Qtaishat, N.M., B. Wiggert, and D.R. Pepperberg. 2005. Interphotoreceptor retinoid-binding protein (IRBP) promotes the release of all-trans retinol from the isolated retina following rhodopsin bleaching illumination. *Exp. Eye. Res.* 81:455–463.

Rattner, A., P.M. Smallwood, and J. Nathans. 2000. Identification and characterization of all-trans-retinol dehydrogenase from photoreceptor outer segments, the visual cycle enzyme that reduces all-trans-retinal to all-trans-retinol. *J. Biol. Chem.* 275:11034–11043.

Ripps, H., N.S. Peachey, X. Xu, S.E. Nozell, S.B. Smith, and G.I. Liou. 2000. The rhodopsin cycle is preserved in IRBP "knockout" mice despite abnormalities in retinal structure and function. *Vis. Neurosci.* 17:97–105.

Saari, J.C., G.G. Garwin, J.P. Van Hooser, and K. Palczewski. 1998. Reduction of all-trans-retinal limits regeneration of visual pigment in mice. *Vision Res.* 38:1325–1333.

Schädel, S.A., M. Heck, D. Maretzki, S. Filipek, D.C. Teller, K. Palczewski, and K.P. Hofmann. 2003. Ligand channeling within a G-protein-coupled receptor. The entry and exit of retinals in native opsin. *J. Biol. Chem.* 278:24896–24903.

Shaw, N.S., and N. Noy. 2001. Interphotoreceptor retinoid-binding protein contains three retinoid binding sites. *Exp. Eye Res.* 72:183–190.

Sherry, D.M., D.D. Bui, and W.J. Degrip. 1998. Identification and distribution of photoreceptor subtypes in the neotenic tiger salamander retina. *Vis. Neurosci.* 15:1175–1187.

Surya, A., K.W. Foster, and B.E. Knox. 1995. Transducin activation by the bovine opsin apoprotein. *J. Biol. Chem.* 270:5024–5031.

Thomas, M.M., and T.D. Lamb. 1999. Light adaptation and dark adaptation of human rod photoreceptors measured from the a-wave of the electroretinogram. *J. Physiol.* 518:479–496.

Tsin, A.T., H.A. Pedrozo-Fernandez, J.M. Gallas, and J.P. Chambers. 1988. The fluorescence quantum yield of vitamin A2. *Life Sci.* 43:1379–1384.

Tsina, E., C. Chen, Y. Koutalos, P. Ala-Laurila, M. Tsacopoulos, B. Wiggert, R.K. Crouch, and M.C. Cornwall. 2004. Physiological and microfluorometric studies of reduction and clearance of retinal in bleached rod photoreceptors. *J. Gen. Physiol.* 124:429–443.

Vanderkooi, G., and M. Sundaralingam. 1970. Biological membrane structure. II. A detailed model for the retinal rod outer segment membrane. *Proc. Natl. Acad. Sci. USA.* 67:233–238.